

# Active Damping in Series Connected Power Modules with Continuous Output Voltage

Research paper

Sabrina Ulmer<sup>\*ID</sup>, Gernot Schullerus<sup>ID</sup>, Ertugrul Sönmez<sup>ID</sup>

Reutlingen University, Reutlingen, Germany

Received: October 23, 2021; Accepted: November 29, 2021

**Abstract:** This paper presents a modular and scalable power electronics concept for motor control with continuous output voltage. In contrast to multilevel concepts, modules with continuous output voltage are connected in series. The continuous output voltage of each module is obtained by using gallium nitride (GaN) high electron motility transistor (HEMT)s as switches inside the modules with a switching frequency in the range between 500 kHz and 1 MHz. Due to this high switching frequency a LC filter is integrated into the module resulting in a continuous output voltage. A main topic of the paper is the active damping of this LC output filter for each module and the analysis of the series connection of the damping behaviour. The results are illustrated with simulations and measurements.

**Keywords:** power electronics • modularity • scalability • GaN • active filter damping

## 1. Introduction

Nowadays, an increasing demand exists for innovative solutions and concepts regarding the electric mobility. One main reason is the high and still increasing need for mobility. This can ultimately be ascribed to two key causes: The stricter regulations concerning diesel vehicle and fine dust motivated by the decreasing availability of fossil fuels as well by the reduction in emissions and fuel consumption of vehicles in the longer-term perspective. Hence, power electronics plays an even more important role for motor control.

Typically, standard motor applications use conventional frequency converters. In these systems, pulse width modulated output voltages are directly applied to the motor phases for controlling the current and thus the torque. This voltage generation strategy results in high frequency components in the voltage and current signals producing a current ripple with negative impact on the operating machine as well as high frequency displacement currents causing a rapid aging of the bearings and electromagnetic compatibility (EMC) issues (Costabile et al., 2007).

Note, that new developments in wide bandgap (WBG) semiconductors and their properties can be used in power electronics design to avoid these issues. The WBG power devices consist of semiconductor materials such as gallium nitride (GaN) and silicon carbide (SiC). One main benefit of these devices is the low switching losses and thus the opportunity to significantly increase the switching frequency (Ding et al., 2019). This results in lower power dissipation and smaller size of components, and it leads to a significantly increased efficiency (Tamura, 2010) when these power devices are used in inverters (Tamura, 2010; Uemoto et al., 2009).

The increased switching frequency of the WBG power devices makes it possible to implement an adequately designed output filter on the power electronics itself to produce a quasi-continuous output voltage at the output terminals instead of a conventional pulse width modulated voltage. By controlling the drive directly with the desired continuous voltage, some of the disadvantages of the currently available systems can be avoided as illustrated in Lautner and Piepenbreier (2016) based on a prototype with 650 V GaN high electron motility transistors (HEMTs).

\* Email: Sabrina.Ulmer@Reutlingen-University.DE

The application in electric mobility (Pinkos and Guo, 2013) highlights the need for modularisation. Modular concepts allow to achieve the high currents required for the drives by connecting modules in parallel. A concept for a parallel connection of power electronics modules based on GaN transistors was proposed in Li et al. (2016).

In addition to high currents there is a demand for high voltages in power electronics. These high voltages can be achieved by using multilevel structures. Different series connected concepts of power converters have been studied so far. However, the complexity of these structures increases with ever additional level. Challenges like control effort and voltage balancing need to be carefully addressed in multilevel structures. The hard-switching system with pulsed output voltages is a common feature of these concepts. In Ulmer et al. (2021a) the high voltages can be achieved by an appropriate series connection concept of power modules. In contrast to concepts from the literature, the continuous output voltage simplifies the series connection.

As mentioned before, the generation of a quasi-continuous output voltage is an essential element in this design. For this purpose, adequately designed filters are integrated into the power electronics module. Considering voltage terminals with LC filters, the main drawback of these filters is its resonance. In particular, at low load currents and even more with open terminals, the damping of these filters is low. The resulting dynamic behaviour of currents and voltages can lead to significant oscillations and/or overshoots, possibly leading to a damage of the power electronics. A filter stage with dissipative damping approach has been introduced in Stubenrauch et al. (2017) to avoid these issues. As this concept increases the losses and suffers from a reduction of the efficiency, active damping concepts are preferable. Therefore, a state feedback of filter state variables such as inductor current or capacitor voltage can be applied to shape the filter transfer characteristic. In Maislinger et al. (2019) an active damping concept for a single module based on the measured capacitor voltage is proposed. A general analysis for active damping of LCL-type output filters is given in Liu et al. (2020).

In Ulmer et al. (2021b) the concept of a three-phase power stage for motor control based on a class-D amplifier operating principle generating a continuous output voltage is introduced. A practically applicable filter design can be achieved by using GaN power semiconductors with switching frequencies in the range between 500 kHz and 1 MHz. Furthermore, the design of an alternative active damping feedback loop of the output filter is developed. In contrast to Maislinger et al. (2019) the active damping is achieved by the filter inductance current feedback. The filter inductance current is used for a state feedback to actively shape the transfer characteristic of the output filter. It is beneficial to use the filter inductance current because this signal can be used for controlling the output current of the module, as well.

In our work a detailed analysis of the behaviour of series connected output filter is presented. The presentation of an active damping approach is an essential component of this work, as well. Simulation results and first measurements are given.

The paper is organised as follows. The next section briefly introduces the modular concept on which the serialisation idea is based. Then, in Section ‘Series Connection of Power Modules with Continuous Output Voltage’ the series connection of power modules with continuous output voltage and its issues are discussed. Next, the active filter damping approach for the series connection of these modules is illustrated in detail in Section ‘Active Damping in Series Connected Power Modules’. Several obtained simulation and measurement results are presented in Sections ‘Simulations’ and ‘Measurements’. Finally, conclusions are given.

## 2. Modular Concept

### 2.1. Unit cell

The modular concept is based on an appropriately designed unit cell with continuous output voltage  $v_o$  and current  $i_o$  based on the transfer characteristic  $H(v_{oRef})$  and a control variable  $v_{oRef}$  illustrated in Figure 1. Here, the unit cell is powered by a DC voltage source,  $V_B$ . Note, that the concept is not limited to DC voltage sources. The basic functionality of a unit cell can be satisfied with the concept of  $\Delta\Sigma$  modulation. The modulator produces a pulsed voltage  $v_{HB}$  which is filtered by an appropriately designed LC output filter. In the current concept, a  $\Delta\Sigma$  modulator produces switching frequencies in a frequency band.

### 2.2. Concept overview

A concept that can be applied for both, parallel and series connection of unit cells, is presented in Ulmer et al. (2019). Due to the continuous output voltage, the unit cell is particularly well suited for scaling the power range to

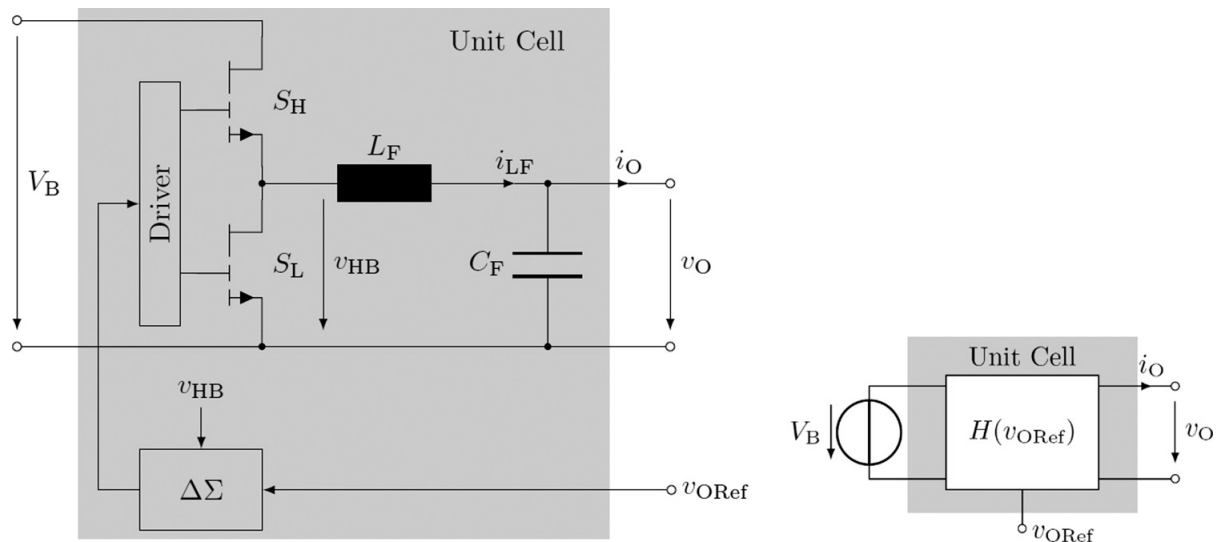


Fig. 1. Internal structure of a unit cell.

the user demands. These hardware modules can be connected in series or in parallel to achieve the requirements with less effort than the conventional solutions. A parallel connection achieves higher output currents. In contrast, a series connection enables higher output voltages. A combination of these two connection concepts is illustrated in Figure 2. The connection principle is based on the parallel connection of 2 unit cells in each case which in turn are connected in series. Note, that for the sake of simplicity only this connection principle is presented here. The extension to additional series or parallel connections is straightforward.

Compared to multilevel topologies, the structure of a unit cell is simplified but the effort for the unit cell itself is increased. Due to the flexible usability and replicability for different applications, the unit cell enables to manufacture in large quantities, thus reducing production and storage costs.

### 2.3. Series connection

In Figure 3 the concept for a series connection of 2 unit cells is illustrated. The extension to several unit cells is straightforward as can be seen in Figure 4 shown by 3 unit cells. The overall output voltage  $v_O$  can be distributed across the unit cells. Note, that the given values  $f_{oi} = 1$  kHz and  $A_{oi} = 24$  V have been arbitrarily selected. The topology is based on the idea that all series connected unit cells are powered by a separate voltage source  $V_{Bi}$ , similar to the signals  $v_{ORef}$  which are galvanically isolated from each other. In an industrial application typically only one power source is connected to the power electronics, whereas in electric vehicles this structure can easily be achieved by connecting the different unit cells to different battery packs. The transfer characteristic  $H(v_{ORef})$  of each unit cell is specified in a way that the unit cell represents a voltage source.

## 3. Series Connection of Power Modules with Continuous Output Voltage

This section analytically describes the behaviour of a LC output filter which is implemented in each unit cell to generate the continuous output voltage. Thereafter, the contents are expanded with the series connection of these unit cells. The derived transfer functions illustrate the need for an active filter damping presented in the following section.

The series connection of 2 unit cells with continuous output voltage is reported for the first time in Ulmer et al. (2021a). Note, that in Ulmer et al. (2021a), inconsistency exists between the figures and the modelling. The given calculations and results don't respond to the figures. The inconsistency is eliminated in this work.

The state space representation used in Section 'Series Connection of Power Modules with Continuous Output Voltage' and 'Active Damping in Series Connected Power Modules' is discussed in detail in Lunze (2020). For the calculation of the transfer functions it is convenient here, to use the state space representation of the system which is stated as follows:

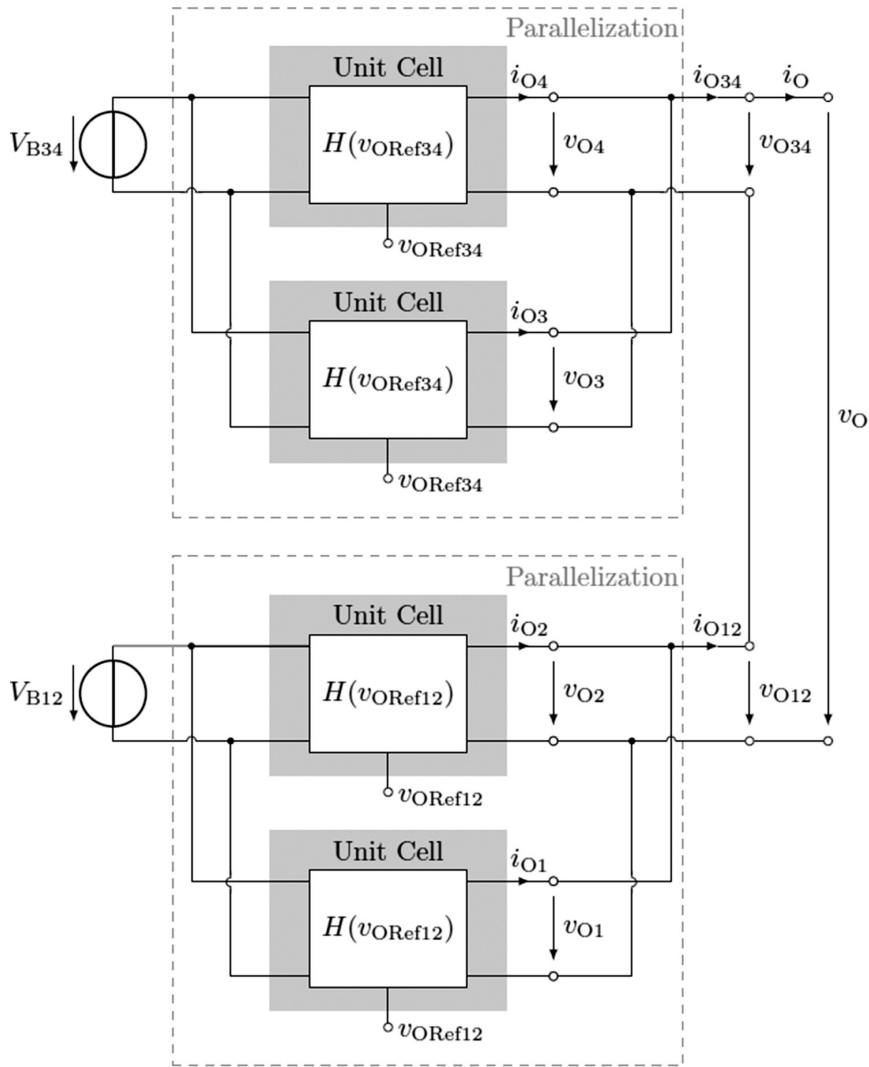


Fig. 2. Parallel and series connection of unit cells.

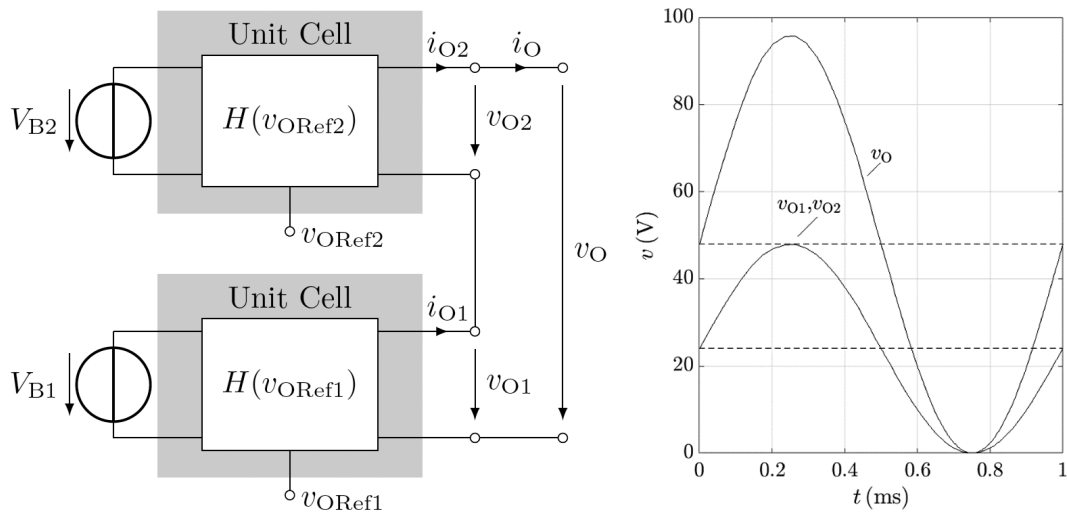


Fig. 3. Series connection of 2 unit cells.

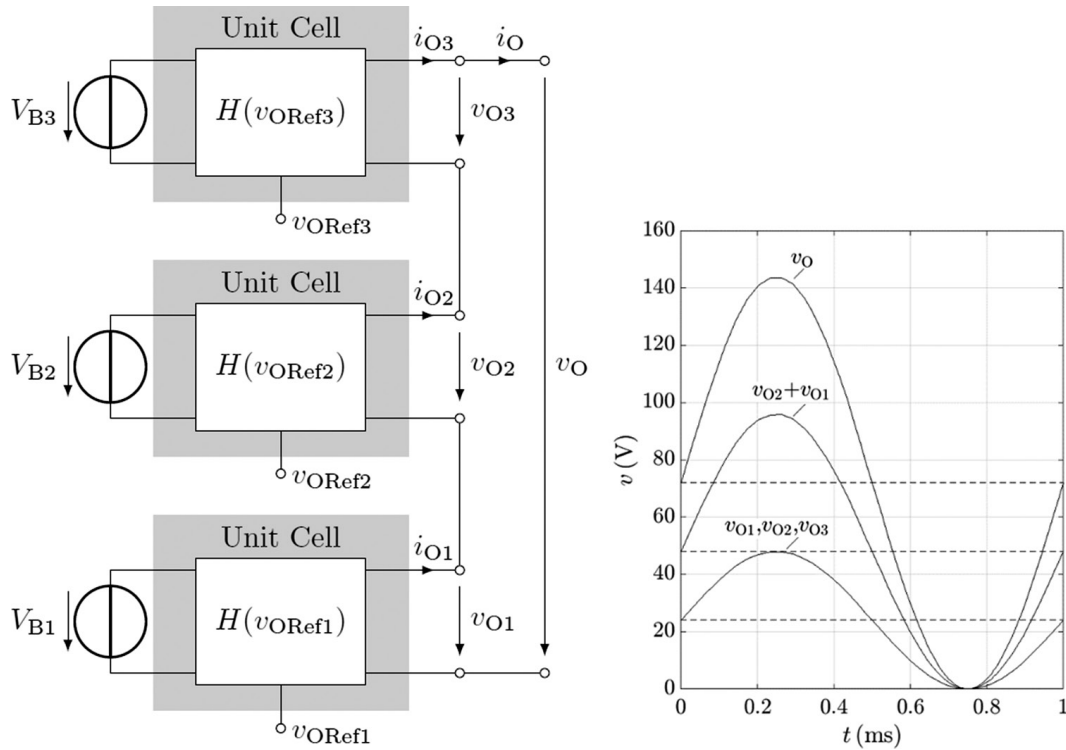


Fig. 4. Series connection of 3 unit cells.

$$\dot{x}(t) = Ax(t) + Bu(t) \tag{1}$$

$$y(t) = Cx(t) + Du(t) \tag{2}$$

$$sX(s) - x_0 = AX(s) + BU(s) \tag{3}$$

$$Y(s) = CX(s) + DU(s) \tag{4}$$

$$\text{for } x_0 = 0 \text{ and } D = 0 \quad \rightarrow \quad G(s) = \frac{Y(s)}{U(s)} = C(sI - A)^{-1}B \tag{5}$$

Note that  $G(s)$  represents the transfer matrix of the system. For determining a particular transfer function, the appropriate row of the matrix  $C$  and the corresponding column of  $B$  are used in Eq. (5).

### 3.1. One unit cell

Based on the internal structure of a unit cell given in Figure 1, Figure 5 illustrates a detailed view of 1 unit cell containing a half-bridge and a passive second-order LC output filter. Depending on the load condition, different state space models will be derived subsequently. Note, that in the equations in the sequel, lower case letter will be used for the voltages and currents to denote the time series.

As the inductor resistance is typically negligible and supposing that no load ( $Z_L \rightarrow \infty$ ) is connected to the LC output filter terminals, the filter dynamics can be modelled by the following state space model:

$$\frac{d}{dt} \begin{bmatrix} i_{LF} \\ v_{CF} \end{bmatrix} = \underbrace{\begin{bmatrix} 0 & -\frac{1}{L_F} \\ \frac{1}{C_F} & 0 \end{bmatrix}}_A \begin{bmatrix} i_{LF} \\ v_{CF} \end{bmatrix} + \underbrace{\begin{bmatrix} \frac{1}{L_F} \\ 0 \end{bmatrix}}_B v_{HB} \tag{6}$$

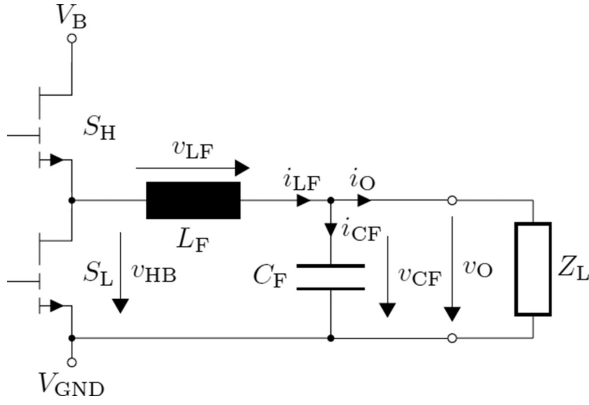


Fig. 5. One unit cell.

The description of the matrices  $A$  and  $B$  referring to Eq. (1) is exemplarily given for Eq. (6) only. The application to the other models is straightforward.

The transfer functions based on Eq. (6) can be expressed in Eqs. (7) and (8) for the unloaded case. To calculate the transfer function for the filter inductor magnitude and the filter capacitor magnitude based on Eqs. (3)–(5), we define as output matrix  $C = [1, 0]$  and  $C = [0, 1]$ . Note, that the detailed expression of the transfer functions based on Eq. (5) is exemplarily given for this condition only. The extension to the other conditions and setups is straightforward.

$$G_{i_{LF}}(s) = \frac{i_{LF}}{v_{HB}} = [1 \quad 0] \frac{1}{s^2 + \frac{1}{L_F C_F}} \begin{bmatrix} s & \frac{1}{L_F} \\ -\frac{1}{C_F} & s \end{bmatrix} \begin{bmatrix} \frac{1}{L_F} \\ 0 \end{bmatrix} = \frac{C_F s}{L_F C_F s^2 + 1} \quad (7)$$

$$G_{v_{CF}}(s) = \frac{v_{CF}}{v_{HB}} = [0 \quad 1] \frac{1}{s^2 + \frac{1}{L_F C_F}} \begin{bmatrix} s & \frac{1}{L_F} \\ -\frac{1}{C_F} & s \end{bmatrix} \begin{bmatrix} \frac{1}{L_F} \\ 0 \end{bmatrix} = \frac{1}{L_F C_F s^2 + 1} \quad (8)$$

Next, supposing that a load  $Z_L$  given by a resistor  $R_L$  is connected to the LC output filter terminals, the filter dynamics is represented by the state space model:

$$\frac{d}{dt} \begin{bmatrix} i_{LF} \\ v_{CF} \end{bmatrix} = \begin{bmatrix} 0 & -\frac{1}{L_F} \\ \frac{1}{C_F} & -\frac{1}{R_L C_F} \end{bmatrix} \begin{bmatrix} i_{LF} \\ v_{CF} \end{bmatrix} + \begin{bmatrix} \frac{1}{L_F} \\ 0 \end{bmatrix} v_{HB} \quad (9)$$

The transfer functions based on Eq. (9) can be expressed in Eqs. (10) and (11) for the resistive loaded case.

$$G_{i_{LF}}(s) = \frac{C_F R_L s + 1}{C_F L_F R_L s^2 + L_F s + R_L} \quad (10)$$

$$G_{v_{CF}}(s) = \frac{R_L}{C_F L_F R_L s^2 + L_F s + R_L} \quad (11)$$

Next, supposing that a load  $Z_L$  is given by a series connection of  $R_M$  and  $L_M$  corresponding to a motor winding is connected to the LC output filter terminals, the filter dynamics is then given by:

$$\frac{d}{dt} \begin{bmatrix} i_{LF} \\ v_{CF} \\ i_O \end{bmatrix} = \begin{bmatrix} 0 & -\frac{1}{L_F} & 0 \\ \frac{1}{C_F} & 0 & -\frac{1}{C_F} \\ 0 & \frac{1}{L_M} & -\frac{R_M}{C_F} \end{bmatrix} \begin{bmatrix} i_{LF} \\ v_{CF} \\ i_O \end{bmatrix} + \begin{bmatrix} \frac{1}{L_F} \\ 0 \\ 0 \end{bmatrix} v_{HB} \quad (12)$$

The transfer functions based on Eq. (12) can be expressed in Eqs. (13)–(15) for the resistive-inductive loaded case.

$$G_{iLF}(s) = \frac{C_F^2 L_M s^2 + C_F L_M R_M s + C_F}{C_F^2 L_F L_M s^3 + C_F L_F L_M R_M s^2 + (C_F L_M + C_F L_F) s + L_M R_M} \quad (13)$$

$$G_{vCF}(s) = \frac{C_F L_M s + L_M R_M}{C_F^2 L_F L_M s^3 + C_F L_F L_M R_M s^2 + (C_F L_M + C_F L_F) s + L_M R_M} \quad (14)$$

$$G_{iO}(s) = \frac{C_F}{C_F^2 L_F L_M s^3 + C_F L_F L_M R_M s^2 + (C_F L_M + C_F L_F) s + L_M R_M} \quad (15)$$

Note, that the DC gain of the output voltage  $v_o$  in Eqs. (8), (11) and (14) is equal to one, which is an expected result. The values of the filter and load components used in the subsequent analysis are given in Table 1.

Figure 6 illustrates the magnitudes of the transfer functions bases on Eqs. (7), (8), (10), (11) and (13)–(15) using the system parameters from Table 1. On the left-hand side, the output voltage has a constant magnitude over a wide frequency range. In the range of the filter resonance a resonance peak occurs which can become an

**Table 1.** Values of the filter and load components

Component		Value	Unit
Filter inductance	$L_F$	15	$\mu\text{H}$
Filter capacitance	$C_F$	1.36	$\mu\text{F}$
Filter resistance (Parasitic)	$R_F$	2.86	$\text{m}\Omega$
Motor inductance	$L_M$	1	$\text{mH}$
Motor resistance	$R_M$	0.4	$\Omega$
Resistive load	$R_L$	4	$\Omega$

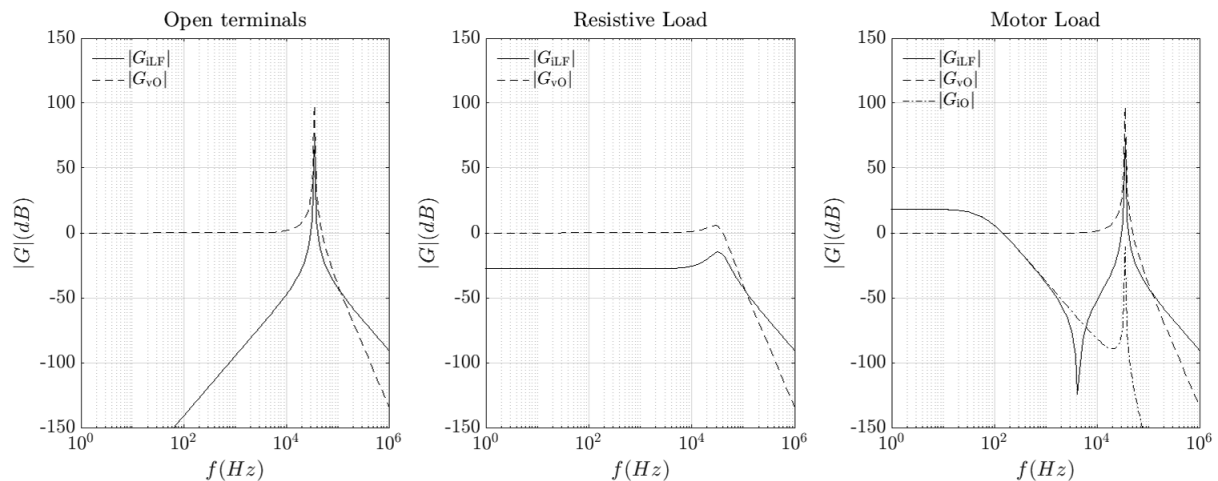


**Fig. 6.** Magnitude response for 1 unit cell.

issue for the output capacitance. The current through the filter inductance strongly increases in the range of the resonance, as well, which is critical as this is the current through the switch. In the centre, the resistive load has a dampening effect, as expected from the passive damping approach in Stubenrauch et al. (2017). In addition, in motor control no pure resistive load is applied. On the right-hand side, all magnitudes of the motor load exhibit the same resonance issues as the unloaded case.

### 3.2. Two unit cells

Figure 7 illustrates a detailed view of two series connected unit cells. Supposing that no load ( $Z_L \rightarrow \infty$ ) is connected to the LC output filter terminals, the filter dynamics can be modelled by the following state space model:

$$\frac{d}{dt} \begin{bmatrix} i_{LF1} \\ i_{LF2} \\ v_{CF1} \\ v_{CF2} \end{bmatrix} = \begin{bmatrix} 0 & 0 & -\frac{1}{L_{F1}} & 0 \\ 0 & 0 & 0 & -\frac{1}{L_{F2}} \\ \frac{1}{C_{F1}} & 0 & 0 & 0 \\ 0 & \frac{1}{C_{F2}} & 0 & 0 \end{bmatrix} \begin{bmatrix} i_{LF1} \\ i_{LF2} \\ v_{CF1} \\ v_{CF2} \end{bmatrix} + \begin{bmatrix} \frac{1}{L_{F1}} & 0 \\ 0 & \frac{1}{L_{F2}} \\ 0 & 0 \\ 0 & 0 \end{bmatrix} \begin{bmatrix} v_{HB1} \\ v_{HB2} \end{bmatrix} \quad (16)$$

The transfer functions based on Eq. (16) can be expressed with  $a = C_{F1}L_{F1}$  and  $b = C_{F2}L_{F2}$  in Eqs. (17) and (18) for the unloaded case. To calculate the transfer function for the filter inductor magnitude and the filter capacitor magnitude based on Eqs. (3)–(5), we define as output matrix  $C = [1,0,0,0]$  and  $C = [0,0,1,1]$ .

$$G_{iLF1}(s) = \frac{C_{F1}s}{as^2 + 1} \quad (17)$$

$$G_{vO}(s) = \frac{1}{as^2 + 1} + \frac{1}{bs^2 + 1} \quad (18)$$

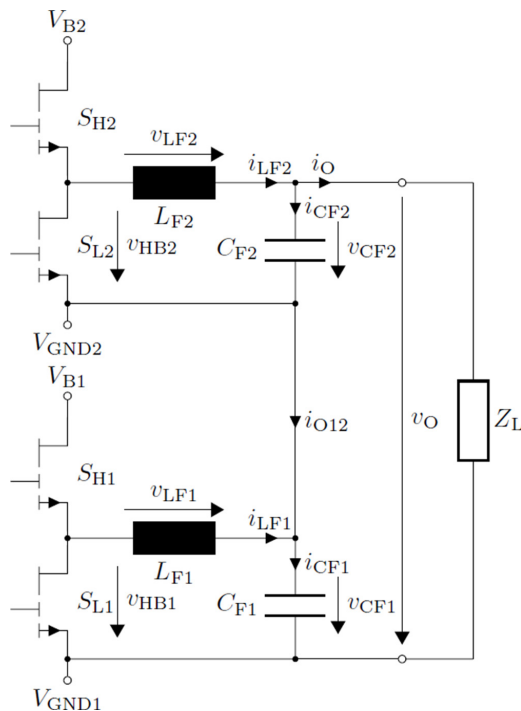


Fig. 7. Two unit cells.

Next, supposing that a load  $Z_L$  given by a resistor  $R_L$  is connected to the LC output filter terminals, the filter dynamics change to the state space model is given below:

$$\frac{d}{dt} \begin{bmatrix} i_{LF1} \\ i_{LF2} \\ v_{CF1} \\ v_{CF2} \end{bmatrix} = \begin{bmatrix} 0 & 0 & -\frac{1}{L_{F1}} & 0 \\ 0 & 0 & 0 & -\frac{1}{L_{F2}} \\ \frac{1}{C_{F1}} & 0 & -\frac{1}{R_L C_{F1}} & -\frac{1}{R_L C_{F1}} \\ 0 & \frac{1}{C_{F2}} & -\frac{1}{R_L C_{F2}} & -\frac{1}{R_L C_{F2}} \end{bmatrix} \begin{bmatrix} i_{LF1} \\ i_{LF2} \\ v_{CF1} \\ v_{CF2} \end{bmatrix} + \begin{bmatrix} \frac{1}{L_{F1}} & 0 \\ 0 & \frac{1}{L_{F2}} \\ 0 & 0 \\ 0 & 0 \end{bmatrix} \begin{bmatrix} v_{HB1} \\ v_{HB2} \end{bmatrix} \quad (19)$$

The transfer functions based on Eq. (19) can be expressed with  $a = C_{F1}L_{F1}$  and  $b = C_{F2}L_{F2}$  in Eqs. (20) and (21) for the resistive loaded case.

$$G_{i_{LF1}}(s) = \frac{bC_{F1}R_Ls^3 + (C_{F2} + C_{F1})L_{F2}s^2 + C_{F1}R_Ls + 2}{abR_Ls^4 + (C_{F2} + C_{F1})L_{F1}L_{F2}s^3 + (a+b)R_Ls^2 + (L_{F2} + L_{F1})s + R_L} \quad (20)$$

$$G_{v_O}(s) = \frac{bR_Ls^2 + aR_Ls^2 + 2R_L}{abR_Ls^4 + (C_{F2} + C_{F1})L_{F1}L_{F2}s^3 + (a+b)R_Ls^2 + (L_{F2} + L_{F1})s + R_L} \quad (21)$$

Next, supposing that a load  $Z_L$  is given by a series connection of  $R_M$  and  $L_M$  corresponding to a motor winding is connected to the LC output filter terminals, the filter dynamics is then given by:

$$\frac{d}{dt} \begin{bmatrix} i_{LF1} \\ i_{LF2} \\ v_{CF1} \\ v_{CF2} \\ i_O \end{bmatrix} = \begin{bmatrix} 0 & 0 & -\frac{1}{L_{F1}} & 0 & 0 \\ 0 & 0 & 0 & -\frac{1}{L_{F2}} & 0 \\ \frac{1}{C_{F1}} & 0 & 0 & 0 & -\frac{1}{C_{F1}} \\ 0 & \frac{1}{C_{F2}} & 0 & 0 & -\frac{1}{C_{F2}} \\ 0 & 0 & \frac{1}{L_M} & \frac{1}{L_M} & -\frac{R_M}{L_M} \end{bmatrix} \begin{bmatrix} i_{LF1} \\ i_{LF2} \\ v_{CF1} \\ v_{CF2} \\ i_O \end{bmatrix} + \begin{bmatrix} \frac{1}{L_{F1}} & 0 \\ 0 & \frac{1}{L_{F2}} \\ 0 & 0 \\ 0 & 0 \\ 0 & 0 \end{bmatrix} \begin{bmatrix} v_{HB1} \\ v_{HB2} \end{bmatrix} \quad (22)$$

The transfer functions based on Eq. (22) can be expressed with  $a = C_{F1}L_{F1}$  and  $b = C_{F2}L_{F2}$  in Eqs. (23)–(25) for the resistive-inductive loaded case.

$$G_{i_{LF1}}(s) = \frac{bC_{F1}L_Ms^4 + bC_{F1}R_Ms^3 + (C_{F1}L_M + (C_{F2} + C_{F1})L_{F2})s^2 + C_{F1}R_Ms + 2}{abL_Ms^5 + abR_Ms^4 + ((a+b)L_M(C_{F2} + C_{F1})L_{F1}L_{F2})s^3 + (a+b)R_Ms^2 + (L_M + L_{F2} + L_{F1})s + R_M} \quad (23)$$

$$G_{v_O}(s) = \frac{bL_Ms^3 + bR_Ms^2 + aL_Ms^3 + aR_Ms^2 + 2L_Ms + 2R_M}{abL_Ms^5 + abR_Ms^4 + ((a+b)L_M(C_{F2} + C_{F1})L_{F1}L_{F2})s^3 + (a+b)R_Ms^2 + (L_M + L_{F2} + L_{F1})s + R_M} \quad (24)$$

$$G_{i_O}(s) = \frac{as^2 + bs^2 + 2}{abL_Ms^5 + abR_Ms^4 + ((a+b)L_M(C_{F2} + C_{F1})L_{F1}L_{F2})s^3 + (a+b)R_Ms^2 + (L_M + L_{F2} + L_{F1})s + R_M} \quad (25)$$

Note, that the DC gain of the output voltage  $v_o$  in Eqs. (18), (21) and (24) is equal to 2. Furthermore, the DC gain of the output current in Eq. (25) is equal to  $2/R$ , which is an expected result.

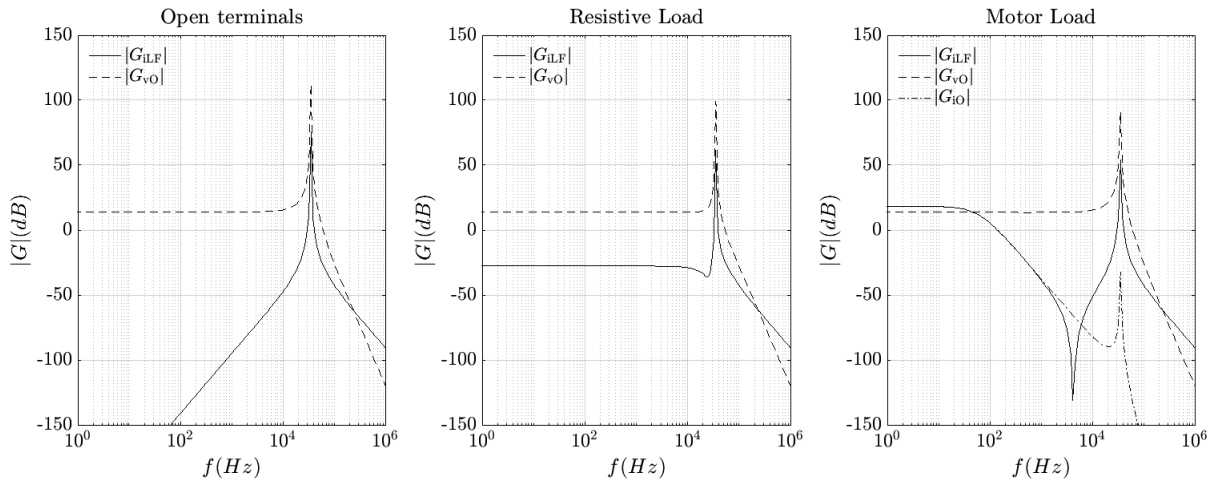


Fig. 8. Magnitude response for 2 unit cells.

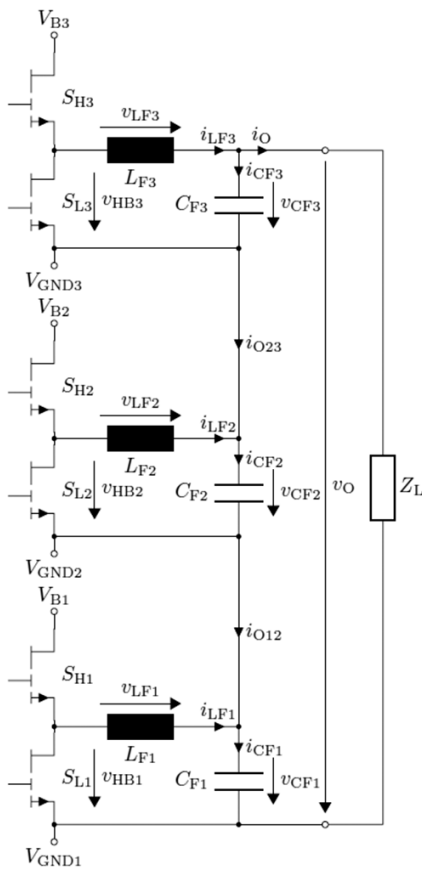


Fig. 9. Three unit cells.

Figure 8 illustrates the magnitudes of the transfer functions based on Eqs. (17), (18), (20), (21) and (23)–(25). On the left-hand side, a similar behaviour as in Figure 6 is recognisable. This also applies for the right-hand side. Only, the resonance peaks of the resistive load are increased.

### 3.3. Three unit cells

Figure 9 illustrates a detailed view of 3 unit cells. Supposing that no load ( $Z_L \rightarrow \infty$ ) is connected to the LC output filter terminals, then the filter dynamics can be modelled by the following state space model:

$$\frac{d}{dt} \begin{bmatrix} i_{LF1} \\ i_{LF2} \\ i_{LF3} \\ v_{CF1} \\ v_{CF2} \\ v_{CF3} \end{bmatrix} = \begin{bmatrix} 0 & 0 & 0 & -\frac{1}{L_{F1}} & 0 & 0 \\ 0 & 0 & 0 & 0 & -\frac{1}{L_{F2}} & 0 \\ 0 & 0 & 0 & 0 & 0 & -\frac{1}{L_{F3}} \\ \frac{1}{C_{F1}} & 0 & 0 & 0 & 0 & 0 \\ 0 & \frac{1}{C_{F2}} & 0 & 0 & 0 & 0 \\ 0 & 0 & \frac{1}{C_{F3}} & 0 & 0 & 0 \end{bmatrix} \begin{bmatrix} i_{LF1} \\ i_{LF2} \\ i_{LF3} \\ v_{CF1} \\ v_{CF2} \\ v_{CF3} \end{bmatrix} + \begin{bmatrix} \frac{1}{L_{F1}} & 0 & 0 \\ 0 & \frac{1}{L_{F2}} & 0 \\ 0 & 0 & \frac{1}{L_{F3}} \\ 0 & 0 & 0 \\ 0 & 0 & 0 \\ 0 & 0 & 0 \end{bmatrix} \begin{bmatrix} v_{HB1} \\ v_{HB2} \\ v_{HB3} \end{bmatrix} \quad (26)$$

The transfer functions based on Eq. (26) can be expressed with  $a = C_{F1}L_{F1}$ ,  $b = C_{F2}L_{F2}$  and  $c = C_{F3}L_{F3}$  in Eqs. (27) and (28) for the unloaded case. To calculate the transfer function for the filter inductor magnitude and the filter capacitor magnitude based on Eqs. (3)–(5), we define as output matrix  $C = [1,0,0,0,0,0]$  and  $C = [0,0,0,1,1,1]$ .

$$G_{i_{LF1}}(s) = \frac{C_{F1}s}{as^2 + 1} \quad (27)$$

$$G_{v_O}(s) = \frac{1}{as^2 + 1} + \frac{1}{bs^2 + 1} + \frac{1}{cs^2 + 1} \quad (28)$$

Next, supposing that a load  $Z_L$  given by a resistor  $R_L$  is connected to the LC output filter terminals, the filter dynamics change to the state space model is given below:

$$\frac{d}{dt} \begin{bmatrix} i_{LF1} \\ i_{LF2} \\ i_{LF3} \\ v_{CF1} \\ v_{CF2} \\ v_{CF3} \end{bmatrix} = \begin{bmatrix} 0 & 0 & 0 & -\frac{1}{L_{F1}} & 0 & 0 \\ 0 & 0 & 0 & 0 & -\frac{1}{L_{F2}} & 0 \\ 0 & 0 & 0 & 0 & 0 & -\frac{1}{L_{F3}} \\ \frac{1}{C_{F1}} & 0 & 0 & -\frac{1}{R_L C_{F1}} & -\frac{1}{R_L C_{F1}} & -\frac{1}{R_L C_{F1}} \\ 0 & \frac{1}{C_{F2}} & 0 & -\frac{1}{R_L C_{F2}} & -\frac{1}{R_L C_{F2}} & -\frac{1}{R_L C_{F2}} \\ 0 & 0 & \frac{1}{C_{F3}} & -\frac{1}{R_L C_{F3}} & -\frac{1}{R_L C_{F3}} & -\frac{1}{R_L C_{F3}} \end{bmatrix} \begin{bmatrix} i_{LF1} \\ i_{LF2} \\ i_{LF3} \\ v_{CF1} \\ v_{CF2} \\ v_{CF3} \end{bmatrix} + \begin{bmatrix} \frac{1}{L_{F1}} & 0 & 0 \\ 0 & \frac{1}{L_{F2}} & 0 \\ 0 & 0 & \frac{1}{L_{F3}} \\ 0 & 0 & 0 \\ 0 & 0 & 0 \\ 0 & 0 & 0 \end{bmatrix} \begin{bmatrix} v_{HB1} \\ v_{HB2} \\ v_{HB3} \end{bmatrix} \quad (29)$$

Next, supposing that a load  $Z_L$  is given by a series connection of  $R_M$  and  $L_M$  corresponding to a motor winding is connected to the LC output filter terminals, the filter dynamics is then given by:

$$\frac{d}{dt} \begin{bmatrix} i_{LF1} \\ i_{LF2} \\ i_{LF3} \\ v_{CF1} \\ v_{CF2} \\ v_{CF3} \\ i_O \end{bmatrix} = \begin{bmatrix} 0 & 0 & 0 & -\frac{1}{L_{F1}} & 0 & 0 & 0 \\ 0 & 0 & 0 & 0 & -\frac{1}{L_{F2}} & 0 & 0 \\ 0 & 0 & 0 & 0 & 0 & -\frac{1}{L_{F3}} & 0 \\ \frac{1}{C_{F1}} & 0 & 0 & 0 & 0 & 0 & -\frac{1}{C_{F1}} \\ 0 & \frac{1}{C_{F2}} & 0 & 0 & 0 & 0 & -\frac{1}{C_{F2}} \\ 0 & 0 & \frac{1}{C_{F3}} & 0 & 0 & 0 & -\frac{1}{C_{F3}} \\ 0 & 0 & 0 & \frac{1}{L_M} & \frac{1}{L_M} & \frac{1}{L_M} & -\frac{R_M}{L_M} \end{bmatrix} \begin{bmatrix} i_{LF1} \\ i_{LF2} \\ i_{LF3} \\ v_{CF1} \\ v_{CF2} \\ v_{CF3} \\ i_O \end{bmatrix} + \begin{bmatrix} \frac{1}{L_{F1}} & 0 & 0 \\ 0 & \frac{1}{L_{F2}} & 0 \\ 0 & 0 & \frac{1}{L_{F3}} \\ 0 & 0 & 0 \\ 0 & 0 & 0 \\ 0 & 0 & 0 \\ 0 & 0 & 0 \end{bmatrix} \begin{bmatrix} v_{HB1} \\ v_{HB2} \\ v_{HB3} \end{bmatrix} \quad (30)$$

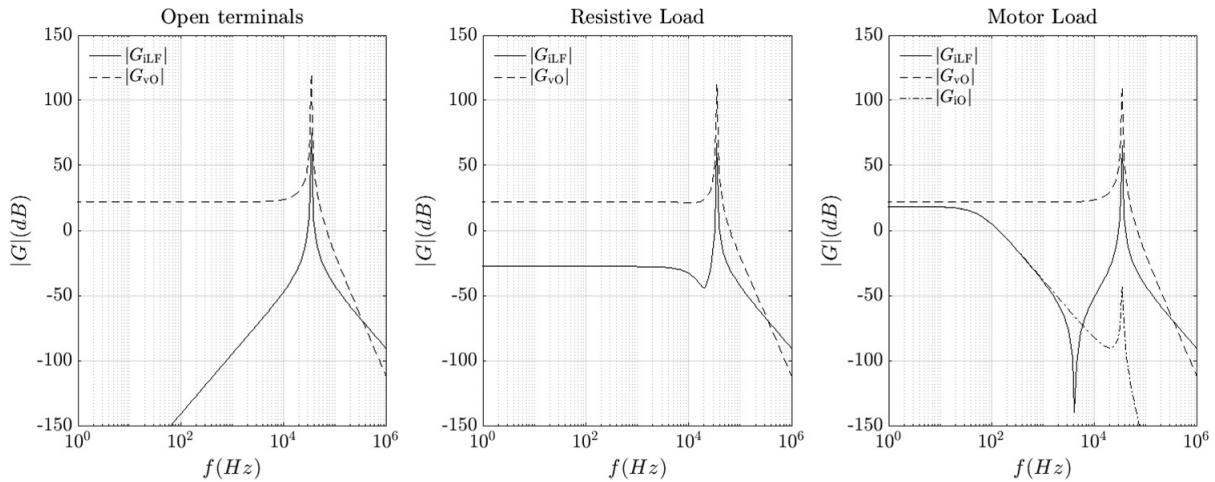


Fig. 10. Magnitude response for 3 unit cells.

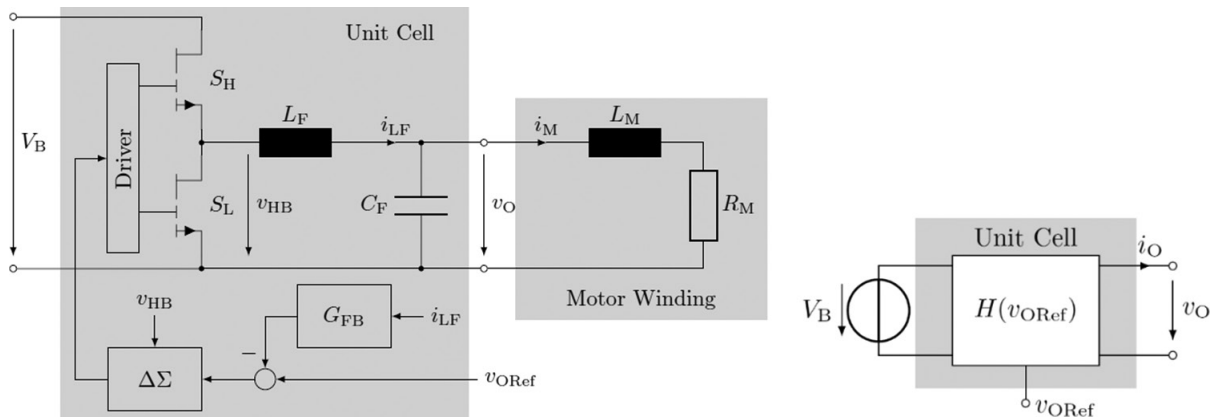


Fig. 11. Internal structure of a unit cell with inductor current feedback.

The transfer functions based on Eqs. (29) and (30) cannot be reasonably expressed in clearly organised terms. Note, that the DC gain of the output voltage  $v_o$  is equal to 3. Furthermore, the DC gain of the output current is equal to  $3/R$ , which is an expected result.

Figure 10 illustrates the magnitudes of the transfer functions based on Eqs. (27) and (28) as well the transfer functions based on the state space models (29) and (30). Compared to Figure 8, no significant changes are recognisable.

## 4. Active Damping in Series Connected Power Modules

As already discussed in Ulmer et al. (2021a) and in the previous section, an active filter damping is important for a safe operation of the unit cell. In contrast to Li et al. (2016), this active damping is achieved by adding a feedback of the inductor current  $i_L$  to the  $\Delta\Sigma$  modulation loop as illustrated in Figure 11. Note, that in the given illustration the motor winding is presented as load.

Depending on the load condition, different state space models will be derived and presented in the following in the sequel. Note, that in the equations in the sequel, lower case letter will be used for the voltages and currents to denote the time series.

In all cases, active damping can be achieved by adding a partial state feedback  $v_{HB} = v_{ORef} - k_{i_{LF}}$  to the existing state space models.

#### 4.1. Active damping of 1 unit cell

Supposing that no load ( $Z_L \rightarrow \infty$ ) is connected to the LC output filter terminals, the filter dynamics can be modelled by the following state space model:

$$\frac{d}{dt} \begin{bmatrix} i_{LF} \\ v_{CF} \end{bmatrix} = \begin{bmatrix} -\frac{k_I}{L_F} & -\frac{1}{L_F} \\ \frac{1}{C_F} & 0 \end{bmatrix} \begin{bmatrix} i_{LF} \\ v_{CF} \end{bmatrix} + \begin{bmatrix} \frac{1}{L_F} \\ 0 \end{bmatrix} v_{ORef} \quad (31)$$

The value of the current feedback gain  $k_I$  is determined by pole placement in such a way that an appropriate damping of the system is achieved. The characteristic polynomial of the system matrix in Eq. (31) is given by:

$$P(s) = s^2 + \frac{k_I}{L_F} s + \frac{1}{L_F C_F} \quad (32)$$

The poles of the system (30) are the zeros of  $P(s) = 0$ . A reasonable choice is the determination of the feedback gain  $k_I$  in such way that the system exhibits two identical poles Ulmer et al. (2021b), that is:

$$P(s) = (s + l)^2 \quad \text{with} \quad l = \frac{1}{\sqrt{L_F C_F}} \quad \text{and} \quad k_I = 2\sqrt{\frac{L_F}{C_F}} \quad (33)$$

The transfer functions based on Eq. (31) can be expressed in Eqs. (34) and (35) for the unloaded case. To calculate the transfer function for the filter inductor magnitude and the filter capacitor magnitude based on Eqs. (3)–(5), we define as output matrix  $C = [1, 0]$  and  $C = [0, 1]$ .

$$G_{iLF}(s) = \frac{C_F s}{L_F C_F s^2 + C_F k_I s + 1} \quad (34)$$

$$G_{vO}(s) = \frac{1}{L_F C_F s^2 + C_F k_I s + 1} \quad (35)$$

Next, supposing that a load  $Z_L$  given by a resistor  $R_L$  is connected to the LC output filter terminals, the filter dynamics change to the state space model is given below:

$$\frac{d}{dt} \begin{bmatrix} i_{LF} \\ v_{CF} \end{bmatrix} = \begin{bmatrix} -\frac{k_I}{L_F} & -\frac{1}{L_F} \\ \frac{1}{C_F} & -\frac{1}{R_L C_F} \end{bmatrix} \begin{bmatrix} i_{LF} \\ v_{CF} \end{bmatrix} + \begin{bmatrix} \frac{1}{L_F} \\ 0 \end{bmatrix} v_{ORef} \quad (36)$$

The transfer functions based on Eq. (36) can be expressed in Eqs. (37) and (38) for the resistive loaded case.

$$G_{iLF}(s) = \frac{C_F R_L s + 1}{L_F C_F R_L s^2 + (C_F R_L k_I + L_F) s + k_I + R_L} \quad (37)$$

$$G_{vO}(s) = \frac{R_L}{L_F C_F R_L s^2 + (C_F R_L k_I + L_F) s + k_I + R_L} \quad (38)$$

Next, supposing that a load  $Z_L$  is given by a series connection of  $R_M$  and  $L_M$  corresponding to a motor winding is connected to the LC output filter terminals, the filter dynamics is then given by:

$$\frac{d}{dt} \begin{bmatrix} i_{LF} \\ v_{CF} \\ i_O \end{bmatrix} = \begin{bmatrix} -\frac{k_I}{L_F} & -\frac{1}{L_F} & 0 \\ \frac{1}{C_F} & 0 & -\frac{1}{C_F} \\ 0 & \frac{1}{L_M} & -\frac{R_M}{C_F} \end{bmatrix} \begin{bmatrix} i_{LF} \\ v_{CF} \\ i_O \end{bmatrix} + \begin{bmatrix} \frac{1}{L_F} \\ 0 \\ 0 \end{bmatrix} v_{ORef} \quad (39)$$

The transfer functions based on Eq. (39) can be expressed in Eqs. (40)–(42) for the resistive-inductive loaded case.

$$G_{iLF}(s) = \frac{C_F^2 L_M s^2 + C_F L_M R_M s + C_F}{C_F^2 L_F L_M s^3 + (C_F^2 L_M k_I + C_F L_F L_M R_M) s^2 + (C_F L_M R_M k_I + C_F L_M + C_F L_F) s + C_F k_I + L_M R_M} \quad (40)$$

$$G_{vO}(s) = \frac{C_F L_M s + L_M R_M}{C_F^2 L_F L_M s^3 + (C_F^2 L_M k_I + C_F L_F L_M R_M) s^2 + (C_F L_M R_M k_I + C_F L_M + C_F L_F) s + C_F k_I + L_M R_M} \quad (41)$$

$$G_{iLF}(s) = \frac{C_F}{C_F^2 L_F L_M s^3 + (C_F^2 L_M k_I + C_F L_F L_M R_M) s^2 + (C_F L_M R_M k_I + C_F L_M + C_F L_F) s + C_F k_I + L_M R_M} \quad (42)$$

Figure 12 illustrates the magnitudes of the transfer functions based on Eqs. (34), (35), (37), (38) and (40)–(42). These transfer functions are compared with the transfer functions in Figure 6. On the left-hand side, the resonance peak of the output voltage does not occur in the range of the filter resonance any longer. Furthermore, the current peak of the filter inductance is strongly damped. On the right-hand side, the resonance peaks are also damped.

Note that in the case of the motor load as well as of the resistive load, the value of the constant magnitude is also damped by a certain factor.

## 4.2. Active damping of two series connected modules

Supposing that no load ( $Z_L \rightarrow \infty$ ) is connected to the LC output filter terminals, the filter dynamics can be modelled by the following state space model:

$$\frac{d}{dt} \begin{bmatrix} i_{LF1} \\ i_{LF2} \\ v_{CF1} \\ v_{CF2} \end{bmatrix} = \begin{bmatrix} -\frac{k_{I1}}{L_{F1}} & 0 & -\frac{1}{L_{F1}} & 0 \\ 0 & -\frac{k_{I2}}{L_{F2}} & 0 & -\frac{1}{L_{F2}} \\ \frac{1}{C_{F1}} & 0 & 0 & 0 \\ 0 & \frac{1}{C_{F2}} & 0 & 0 \end{bmatrix} \begin{bmatrix} i_{LF1} \\ i_{LF2} \\ v_{CF1} \\ v_{CF2} \end{bmatrix} + \begin{bmatrix} \frac{1}{L_{F1}} & 0 \\ 0 & \frac{1}{L_{F2}} \\ 0 & 0 \\ 0 & 0 \end{bmatrix} \begin{bmatrix} v_{ORef1} \\ v_{ORef2} \end{bmatrix} \quad (43)$$

The transfer functions based on Eq. (43) can be expressed in Eqs. (44) and (45) for the unloaded case.

$$G_{iLF1}(s) = \frac{C_{F1} s}{C_{F1} L_{F1} s^2 + C_{F1} k_{I1} s + 1} \quad (44)$$

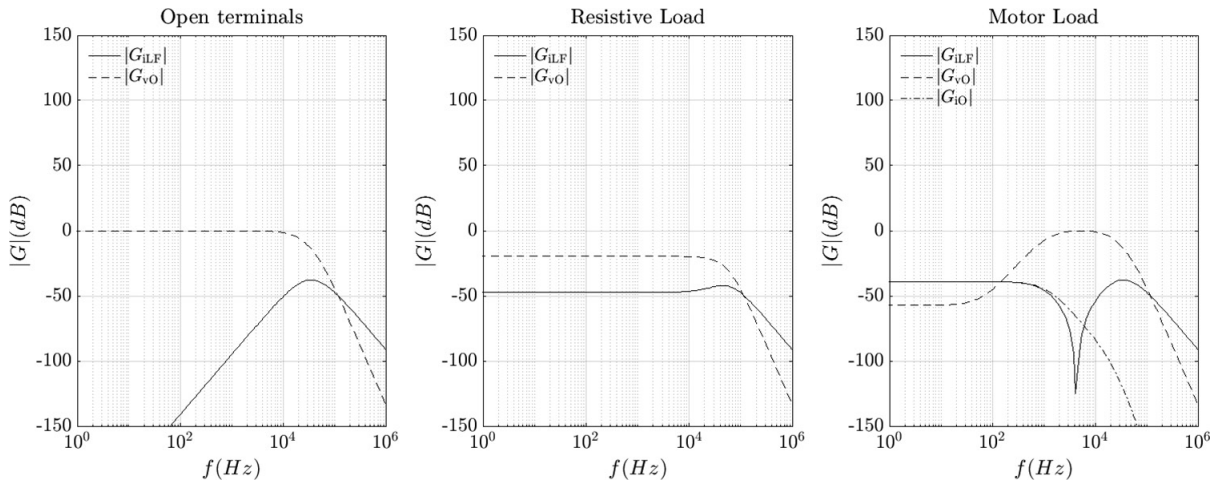


Fig. 12. Magnitude response for 1 unit cell.

$$G_{vO}(s) = \frac{1}{C_{F1}L_{F1}s^2 + C_{F1}k_{I1}s + 1} \frac{L_{F1}}{C_{F2}L_{F1}L_{F2}s^2 + C_{F2}L_{F2}k_{I2}s + L_{F1}} \quad (45)$$

Next, supposing that a load  $Z_L$  given by a resistor  $R_L$  is connected to the LC output filter terminals, the filter dynamics change to the state space model is given below:

$$\frac{d}{dt} \begin{bmatrix} i_{LF1} \\ i_{LF2} \\ v_{CF1} \\ v_{CF2} \end{bmatrix} = \begin{bmatrix} -\frac{k_{I1}}{L_{F1}} & 0 & -\frac{1}{L_{F1}} & 0 \\ 0 & -\frac{k_{I2}}{L_{F2}} & 0 & -\frac{1}{L_{F2}} \\ \frac{1}{C_{F1}} & 0 & -\frac{1}{R_L C_{F1}} & -\frac{1}{R_L C_{F1}} \\ 0 & \frac{1}{C_{F2}} & -\frac{1}{R_L C_{F2}} & -\frac{1}{R_L C_{F2}} \end{bmatrix} \begin{bmatrix} i_{LF1} \\ i_{LF2} \\ v_{CF1} \\ v_{CF2} \end{bmatrix} + \begin{bmatrix} \frac{1}{L_{F1}} & 0 \\ 0 & \frac{1}{L_{F2}} \\ 0 & 0 \\ 0 & 0 \end{bmatrix} \begin{bmatrix} v_{ORef1} \\ v_{ORef2} \end{bmatrix} \quad (46)$$

Next, supposing that a load  $Z_L$  is given by a series connection of  $R_M$  and  $L_M$  corresponding to a motor winding is connected to the LC output filter terminals, the filter dynamics is then given by:

$$\frac{d}{dt} \begin{bmatrix} i_{LF1} \\ i_{LF2} \\ v_{CF1} \\ v_{CF2} \\ i_O \end{bmatrix} = \begin{bmatrix} -\frac{k_{I1}}{L_{F1}} & 0 & -\frac{1}{L_{F1}} & 0 & 0 \\ 0 & -\frac{k_{I2}}{L_{F2}} & 0 & -\frac{1}{L_{F2}} & 0 \\ \frac{1}{C_{F1}} & 0 & 0 & 0 & -\frac{1}{C_{F1}} \\ 0 & \frac{1}{C_{F2}} & 0 & 0 & -\frac{1}{C_{F2}} \\ 0 & 0 & \frac{1}{L_M} & \frac{1}{L_M} & -\frac{R_M}{L_M} \end{bmatrix} \begin{bmatrix} i_{LF1} \\ i_{LF2} \\ v_{CF1} \\ v_{CF2} \\ i_O \end{bmatrix} + \begin{bmatrix} \frac{1}{L_{F1}} & 0 \\ 0 & \frac{1}{L_{F2}} \\ 0 & 0 \\ 0 & 0 \\ 0 & 0 \end{bmatrix} \begin{bmatrix} v_{ORef1} \\ v_{ORef2} \end{bmatrix} \quad (47)$$

The transfer functions based on Eqs. (46) and (47) cannot be reasonably expressed in clearly organised terms. Figure 13 illustrates the magnitudes of the transfer functions based on Eqs. (44) and (45), as well the transfer functions based on the state space models (46) and (47). On the left-hand side, the same behaviour as in Figure 12 is recognisable. This also applies for the right-hand side. Only, the negative resonance peak of the current through

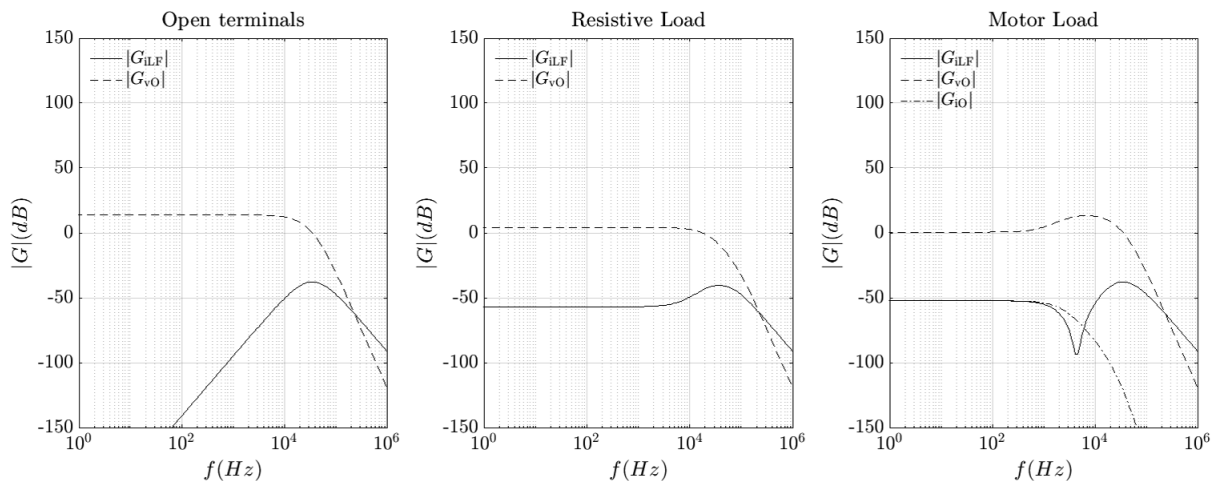


Fig. 13. Magnitude response for 2 unit cells.

the filter inductance is decreased. In addition, the constant value of the output voltage magnitude is increased slightly for the resistive load, as well as for the motor load.

### 4.3. Active damping of three series connected modules

Supposing that no load ( $Z_L \rightarrow \infty$ ) is connected to the LC output filter terminals, the filter dynamics can be modelled by the following state space model:

$$\frac{d}{dt} \begin{bmatrix} i_{LF1} \\ i_{LF2} \\ i_{LF3} \\ v_{CF1} \\ v_{CF2} \\ v_{CF3} \end{bmatrix} = \begin{bmatrix} -\frac{k_{I1}}{L_{F1}} & 0 & 0 & -\frac{1}{L_{F1}} & 0 & 0 \\ 0 & -\frac{k_{I2}}{L_{F2}} & 0 & 0 & -\frac{1}{L_{F2}} & 0 \\ 0 & 0 & -\frac{k_{I3}}{L_{F3}} & 0 & 0 & -\frac{1}{L_{F3}} \\ \frac{1}{C_{F1}} & 0 & 0 & 0 & 0 & 0 \\ 0 & \frac{1}{C_{F2}} & 0 & 0 & 0 & 0 \\ 0 & 0 & \frac{1}{C_{F3}} & 0 & 0 & 0 \end{bmatrix} \begin{bmatrix} i_{LF1} \\ i_{LF2} \\ i_{LF3} \\ v_{CF1} \\ v_{CF2} \\ v_{CF3} \end{bmatrix} + \begin{bmatrix} \frac{1}{L_{F1}} & 0 & 0 \\ 0 & \frac{1}{L_{F2}} & 0 \\ 0 & 0 & \frac{1}{L_{F3}} \\ 0 & 0 & 0 \\ 0 & 0 & 0 \\ 0 & 0 & 0 \end{bmatrix} \begin{bmatrix} v_{ORef1} \\ v_{ORef2} \\ v_{ORef3} \end{bmatrix} \quad (48)$$

Next, supposing that a load  $Z_L$  given by a resistor  $R_L$  is connected to the LC output filter terminals, the filter dynamics change to the state space model is represented by:

$$\frac{d}{dt} \begin{bmatrix} i_{LF1} \\ i_{LF2} \\ i_{LF3} \\ v_{CF1} \\ v_{CF2} \\ v_{CF3} \end{bmatrix} = \begin{bmatrix} -\frac{k_{I1}}{L_{F1}} & 0 & 0 & -\frac{1}{L_{F1}} & 0 & 0 \\ 0 & -\frac{k_{I2}}{L_{F2}} & 0 & 0 & -\frac{1}{L_{F2}} & 0 \\ 0 & 0 & -\frac{k_{I3}}{L_{F3}} & 0 & 0 & -\frac{1}{L_{F3}} \\ \frac{1}{C_{F1}} & 0 & 0 & -\frac{1}{R_L C_{F1}} & -\frac{1}{R_L C_{F1}} & -\frac{1}{R_L C_{F1}} \\ 0 & \frac{1}{C_{F2}} & 0 & -\frac{1}{R_L C_{F2}} & -\frac{1}{R_L C_{F2}} & -\frac{1}{R_L C_{F2}} \\ 0 & 0 & \frac{1}{C_{F3}} & -\frac{1}{R_L C_{F3}} & -\frac{1}{R_L C_{F3}} & -\frac{1}{R_L C_{F3}} \end{bmatrix} \begin{bmatrix} i_{LF1} \\ i_{LF2} \\ i_{LF3} \\ v_{CF1} \\ v_{CF2} \\ v_{CF3} \end{bmatrix} + \begin{bmatrix} \frac{1}{L_{F1}} & 0 & 0 \\ 0 & \frac{1}{L_{F2}} & 0 \\ 0 & 0 & \frac{1}{L_{F3}} \\ 0 & 0 & 0 \\ 0 & 0 & 0 \\ 0 & 0 & 0 \end{bmatrix} \begin{bmatrix} v_{ORef1} \\ v_{ORef2} \\ v_{ORef3} \end{bmatrix} \quad (49)$$

Next, supposing that a load  $Z_L$  is given by a series connection of  $R_M$  and  $L_M$  corresponding to a motor winding is connected to the LC output filter terminals, The filter dynamics is then given by:

$$\frac{d}{dt} \begin{bmatrix} i_{LF1} \\ i_{LF2} \\ i_{LF3} \\ v_{CF1} \\ v_{CF2} \\ v_{CF3} \\ i_O \end{bmatrix} = \begin{bmatrix} -\frac{k_{I1}}{L_{F1}} & 0 & 0 & -\frac{1}{L_{F1}} & 0 & 0 & 0 \\ 0 & -\frac{k_{I2}}{L_{F2}} & 0 & 0 & -\frac{1}{L_{F2}} & 0 & 0 \\ 0 & 0 & -\frac{k_{I3}}{L_{F3}} & 0 & 0 & -\frac{1}{L_{F3}} & 0 \\ \frac{1}{C_{F1}} & 0 & 0 & 0 & 0 & 0 & -\frac{1}{C_{F1}} \\ 0 & \frac{1}{C_{F2}} & 0 & 0 & 0 & 0 & -\frac{1}{C_{F2}} \\ 0 & 0 & \frac{1}{C_{F3}} & 0 & 0 & 0 & -\frac{1}{C_{F3}} \\ 0 & 0 & 0 & \frac{1}{L_M} & \frac{1}{L_M} & \frac{1}{L_M} & -\frac{R_M}{L_M} \end{bmatrix} \begin{bmatrix} i_{LF1} \\ i_{LF2} \\ i_{LF3} \\ v_{CF1} \\ v_{CF2} \\ v_{CF3} \\ i_O \end{bmatrix} + \begin{bmatrix} \frac{1}{L_{F1}} & 0 & 0 \\ 0 & \frac{1}{L_{F2}} & 0 \\ 0 & 0 & \frac{1}{L_{F3}} \\ 0 & 0 & 0 \\ 0 & 0 & 0 \\ 0 & 0 & 0 \\ 0 & 0 & 0 \end{bmatrix} \begin{bmatrix} v_{ORef1} \\ v_{ORef2} \\ v_{ORef3} \end{bmatrix} \quad (50)$$

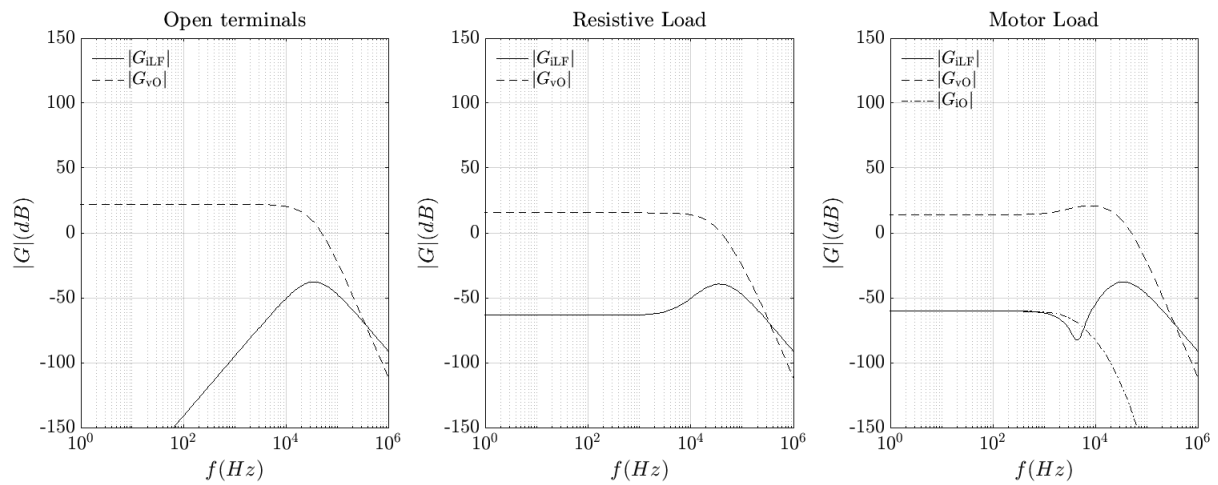


Fig. 14. Magnitude response for 3 unit cells.

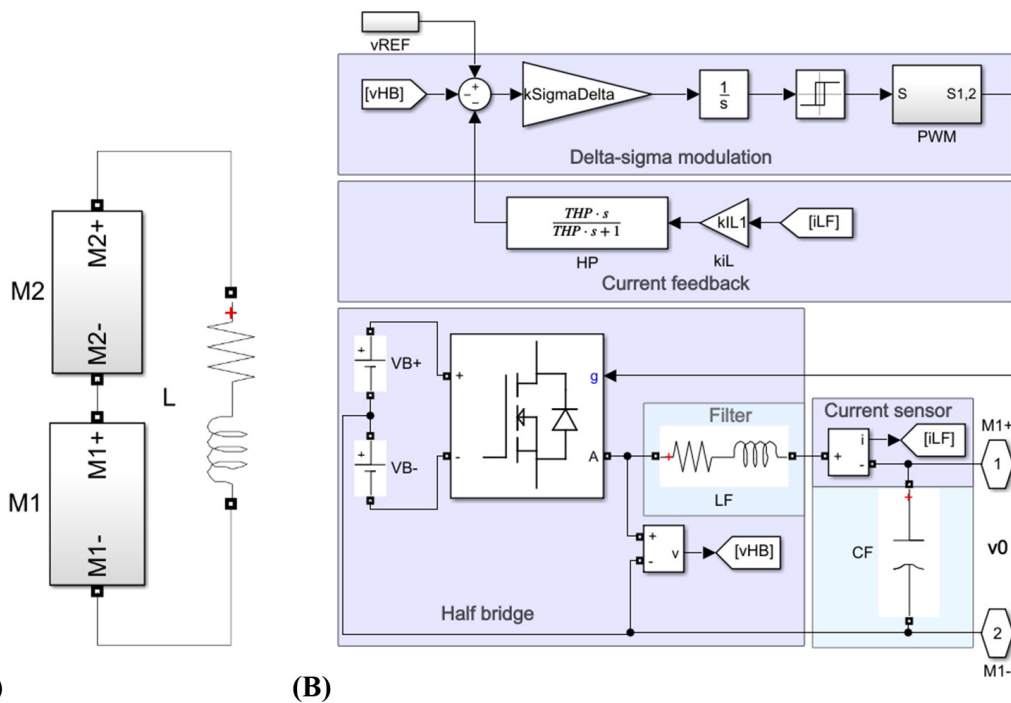


Fig. 15. (A) Simulink model of the top level. (B) Simulink model of the unit cell.

The transfer functions based on Eqs. (48)–(50) cannot be reasonably expressed in clearly organised terms. Figure 14 illustrates the magnitudes of the transfer functions based on the state space models (48)–(50). Compared to Figure 13 no significant changes are observed.

## 5. Simulations

In this section, simulation results are given for a series connection of two modules with the output voltages  $v_{o1}$  and  $v_{o2}$  and the overall output voltage  $v_o$  as illustrated in Figure 15A. The extension to the series connection of several cells is straightforward. A motor winding is presented to the series connected modules.

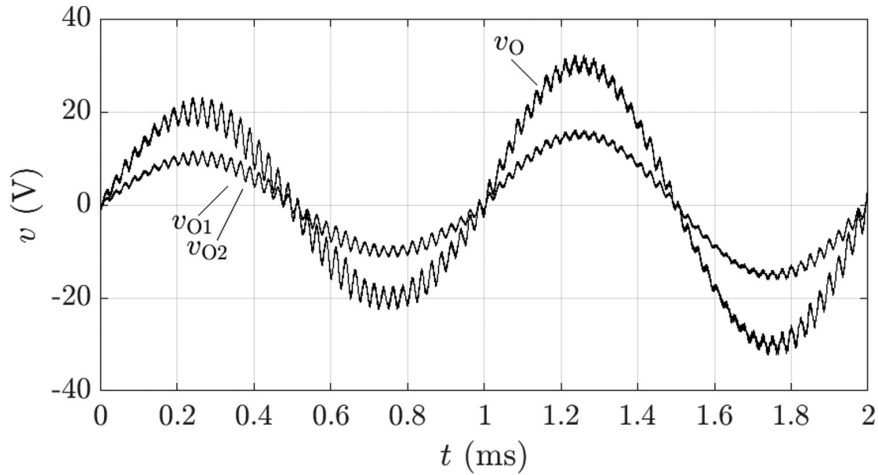


Fig. 16. Simulation results for the undamped output voltages of 2 unit cells with open terminals.

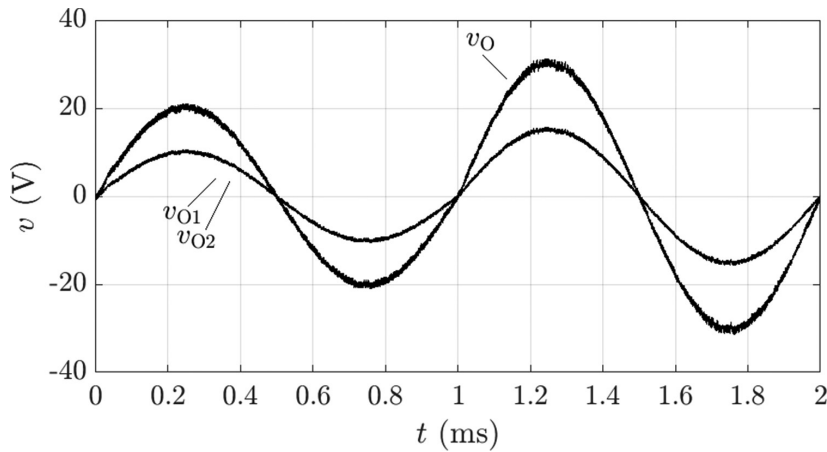


Fig. 17. Simulation results for the damped output voltages of 2 unit cells with open terminals.

The simulation model of the unit cell itself is presented in Figure 15B. Note, that in contrast to the structure in Figure 1, the power supply of the unit cell is split into the voltage source  $V_{B+}$  and  $V_{B-}$  to obtain an output voltage with zero DC offset. In the current feedback loop a high-pass is introduced.

Figures 16–19 illustrate the simulation results for the output voltage  $v_o$  of the series connection of the two module output voltages  $v_{O1}$  and  $v_{O2}$ . The figures differ only in the selection between open terminals (Figures 16 and 17) and motor load (Figures 18 and 19). The same sinusoidal reference voltage  $v_{REF}$  is applied to each module  $M_1$  and  $M_2$ . At  $t = 1\text{ms}$  the amplitude of the reference voltage is increased stepwise in each figure. The effect of damping with  $k_1 = 0$  (Figures 16 and 18) and  $k_1 = k_{IL}$  (Figures 17 and 19) can be observed in the output voltages on comparing Figures 16 with Figure 17 and Figure 18 with Figure 19.

## 6. Measurements

The hardware setup with two and three unit cells connected in series is illustrated in Figure 20. The stacked unit cells have isolated power supplies and isolated input signals, as well. Each unit cell is supplied with  $V_{BI} = 48\text{V}$ .

Figure 21 shows the output voltage  $v_o$  and current  $i_o$  of two series connected unit cells based on the concept in Figure 3. By comparison, Figure 22 shows the output voltage  $v_o$  and current  $i_o$  of three series connected unit cells based on the concept in Figure 4.

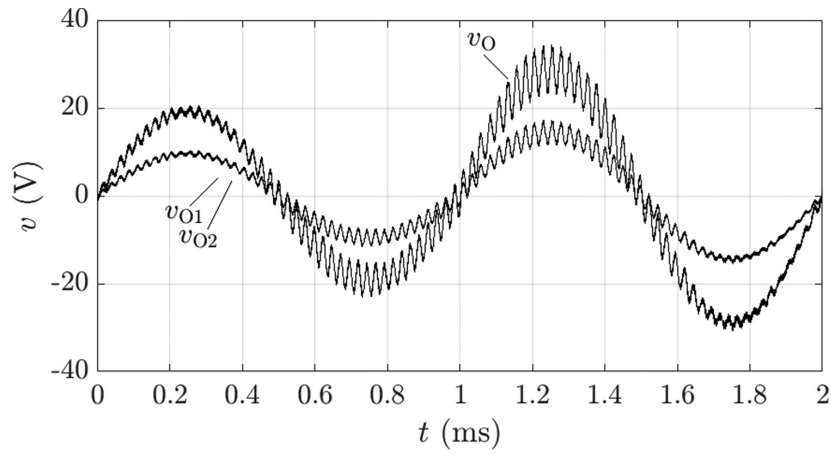


**Fig. 18.** Simulation results for the undamped output voltages of 2 unit cells with motor load.

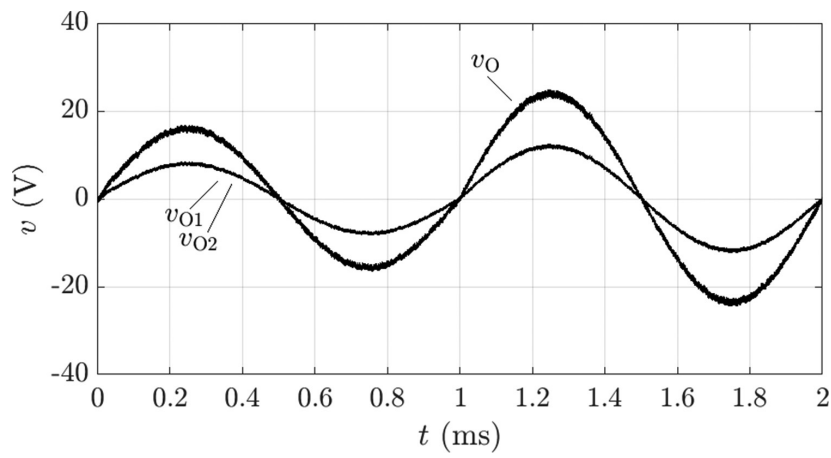


**Fig. 19.** Simulation results for the damped output voltages of 2 unit cells with motor load.

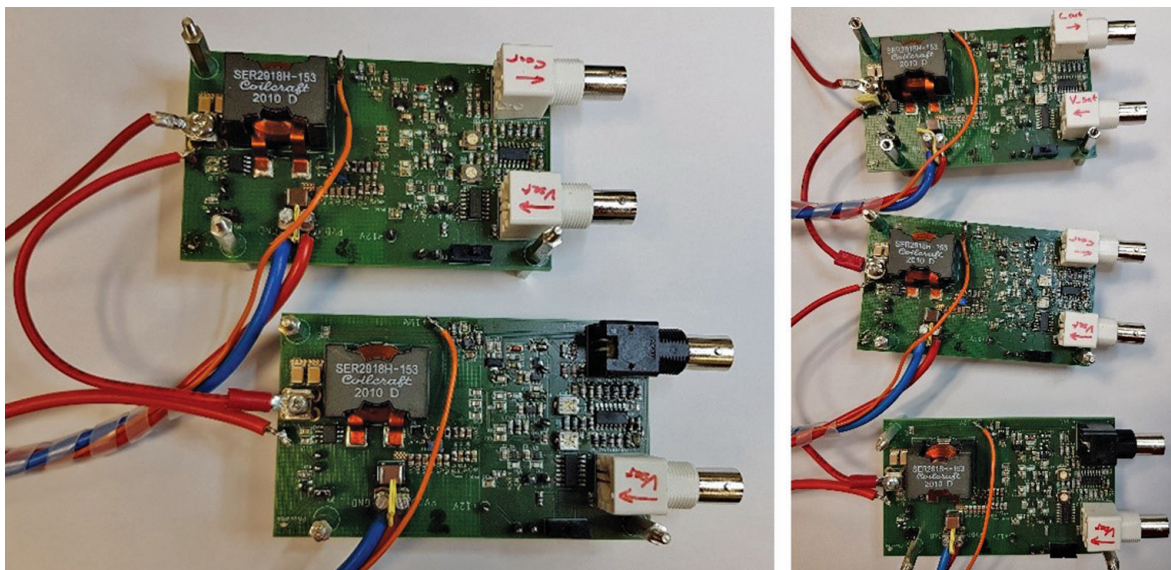


**Fig. 20.** Hardware setup: Two series connected unit cells (left) and three series connected unit cells (right).

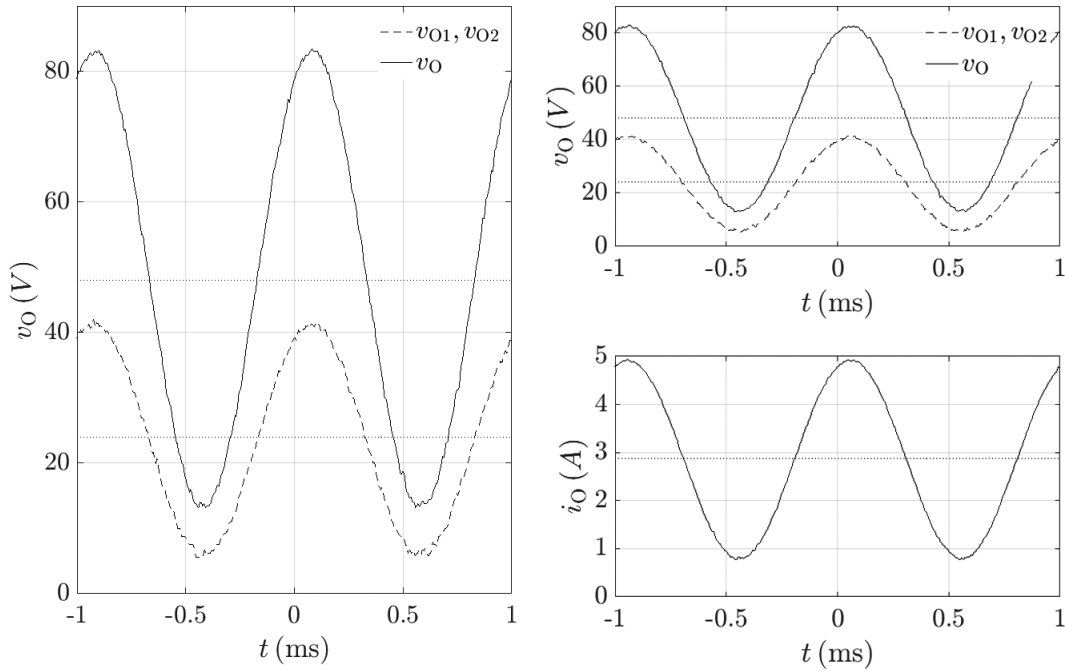


**Fig. 21.** Output voltage and current of two series connected unit cells: Unloaded (left) and loaded with  $16.6 \Omega$  (right).

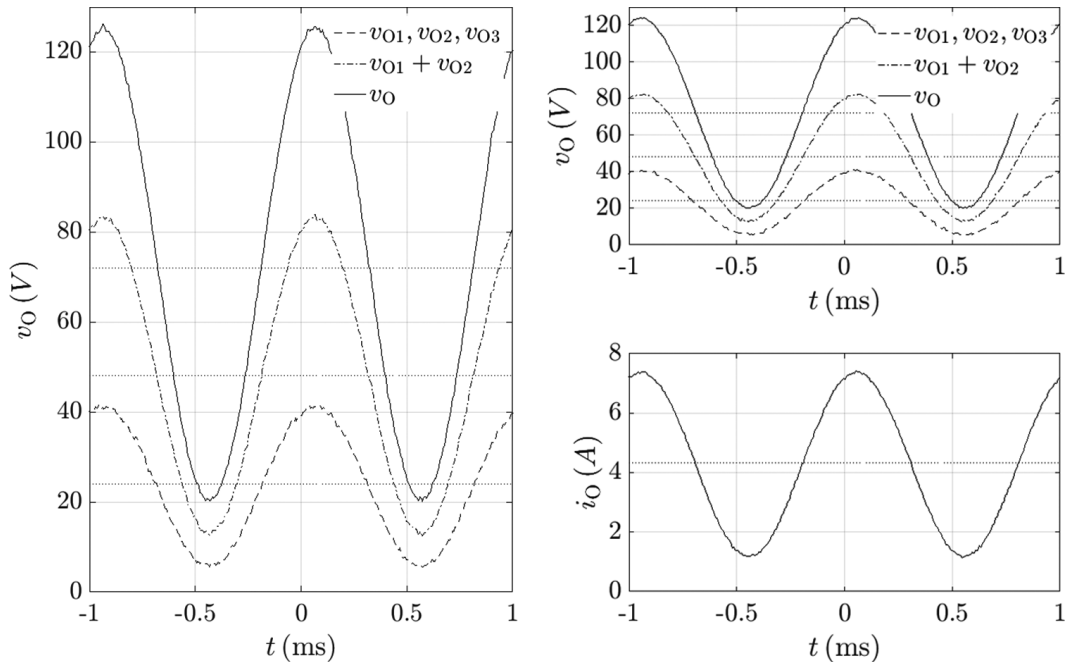


**Fig. 22.** Output voltage and current of three series connected unit cells: Unloaded (left) and loaded with  $16.6 \Omega$  (right).

In Figure 21 on the left-hand side, the system is not connected to a load. Each unit cell generates equal output voltages  $v_{O1}$  and  $v_{O2}$ , which can be measured between the cell's output terminals. It is possible to reach an amplitude of 17 V. The overall output voltage  $v_O$  is referenced to the common ground level. There, an amplitude of about 34 V is achievable due to the serialisation. On the right-hand side, the system is connected to a resistive load of  $16.6 \Omega$ . The amplitude of the output current  $i_O$  is 2 A with respect to the DC offset of 2.9 A. As expected, no difference in the output voltages compared to the left-hand side plot is observed.

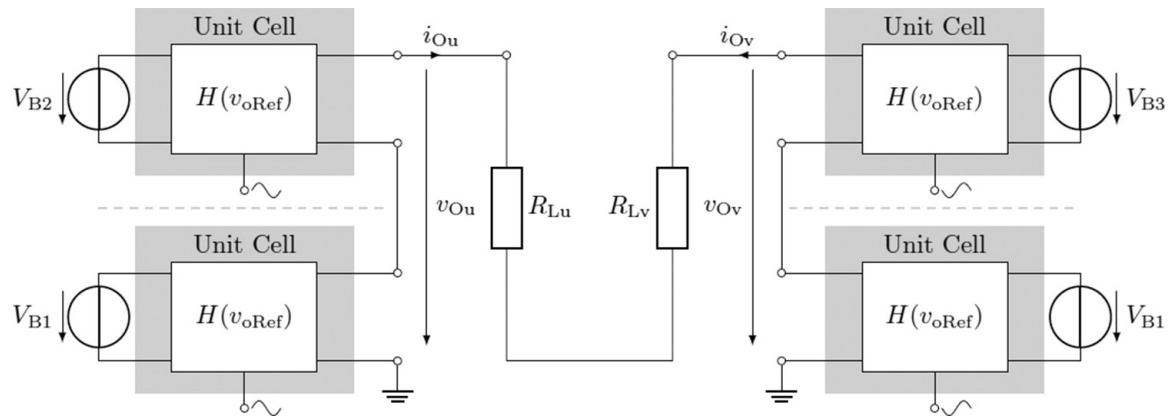


Fig. 23. Two-phase system with two series connected unit cells in each phase.

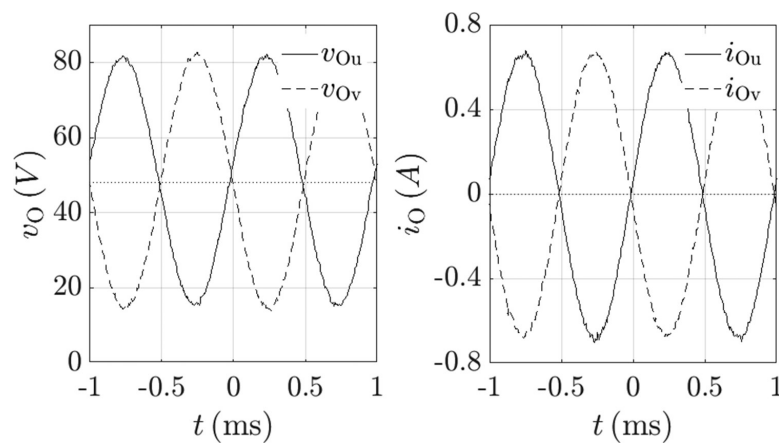


Fig. 24. Output voltages and currents of a two phase system with two series connected unit cells in each phase.

In Figure 22 on the left-hand side, the system is also not connected to a load. Each unit cell connected in series generates equal output voltage  $v_{O1}$ ,  $v_{O2}$ , and  $v_{O3}$ . For the overall output voltage  $v_O$ , it is possible to generate an amplitude of 51 V. On the right-hand side, the system is connected to a resistive load of  $16.6 \Omega$ . The amplitude of the output current  $i_O$  is 3.2 A with respect to the DC offset of 4.2 A. The output voltages of the two load cases don't show any difference.

Due to the number of unit cells for a three-phase system, a motor control setup cannot be presented here. However, a two-phase system with two series connected unit cells in each phase with resistive load is already available. The basic concept is illustrated in Figure 23. There, 2 unit cells share the same voltage source  $V_{B1}$ . The control variable  $v_{ORef}$  for these unit cells is a sinusoidal signal. In case of the phase  $v$ , a phase shift of  $180^\circ$  is added. Each phase, that is,  $u$  and  $v$  has an additional unit cell connected in series. It is important that isolated voltage sources  $V_{B2}$  and  $V_{B3}$  as well as isolated control variables  $v_{ORef2}$  and  $v_{ORef3}$  are applied. The measurement results of the output voltages  $v_{Ou}$  and  $v_{Ov}$  and currents  $i_{Ou}$  and  $i_{Ov}$  are shown in Figure 24.

## Conclusion

This paper illustrates an active damping approach for series connected power modules with continuous output voltage for motor control. The active damping is achieved by the feedback of the inductor current in each LC output filter of the modules.

A detailed discussion regarding the resonance of the output LC filter in the undamped system and the influence of the active damping approach based on a state space representation and transfer functions is presented. The simulation and measurement results illustrate the positive effect of the active damping for each cell. In addition, it is shown that actively damped modules can be connected in series while maintaining a good damping behaviour.

In future work the measurement results will be extended to a three-phase system for motor control with at least 2 unit cells in each phase. Furthermore, the system design of the high pass will be analysed in detail. Keeping the modularisation in mind, the active damping for parallel connected unit cells as well as parallel and series connected unit cells has to be considered.

## Acknowledgments

This work is supported by the German Federal Ministry of Education and Research in the project “Modular Scalable Power Electronics Based on Gallium Nitride with Continuous Output Voltage for Electric Mobility (SkalModEI)”.

## References

- Costabile, G., De Vivo, B., Egiziano, L., Tucci V., Vitelli, M., Beneduce, L., Iovieno, S. and Masucci, A. (2007). An Accurate Evaluation of Electric Discharge Machining Bearings Currents in Inverter-Driven Induction Motors. In: *European Conference on Power Electronics and Applications*, Aalborg, Denmark.
- Ding, X., Zhou, Y. and Cheng, J. (2019). A Review of Gallium Nitride Power Device and Its Applications in Motor Drive. *CES Transactions on Electrical Machines and Systems*, 3(1), pp. 54–64.
- Lautner, J. and Piepenbreier B. (2016). High Efficiency Three-Phase-Inverter with 650 V GaN HEMTs. In: *International Exhibition and Conference for Power Electronics, Intelligent Motion, Renewable Energy and Energy Management*, Nuremberg, Germany.
- Li, H., Zhang, X., Wen, L., Brothers, J.A., Yao, C., Zhu, K., Wang, J., Liu, L., Xu, J. and Puukko, J. (2016) Evaluation of High Voltage Cascode GaN HEMTs in Parallel Operation. In: *IEEE Applied Power Electronics Conference and Exposition*, Long Beach, CA, USA.
- Liu, T., Liu, J. and Liu, Z. (2020). A Study of Virtual Resistor-Based Active Damping Alternatives for LCL Resonance in Grid-Connected Voltage Source Inverters. *IEEE Transactions on Power Electronics*, 35(1), pp. 247–262.
- Lunze, J. (2020). *Regelungstechnik 2: Mehrgrößensysteme, Digitale Regelung*. Springer Vieweg, 10th ed., vol. 2, Berlin, Heidelberg.
- Maislinger, F., Ertl, H., Stojcic, G., Lagler, C. and Holzner, F. (2019). Design of a 100 kHz Wide Bandgap Inverter for Motor Applications with Active Damped Sine Wave Filter. *The Journal of Engineering*, 2019(17), pp. 3766–3771.
- Pinkos, A. F. and Guo, Y. (2013). Automotive Design Challenges for Wide-Band-Gap Devices Used in High Temperature Capable, Scalable Power Vehicle Electronics. In: *IEEE Energytech*, Cleveland, OH, USA.
- Stubenrauch, F., Seliger, N. and Schmitt-Landsiedel, D. (2017). Design and Performance of a 200 kHz GaN Motor Inverter with Sine Wave Filter. In: *International Exhibition and Conference for Power Electronics, Intelligent Motion, Renewable Energy and Energy Management*, Nuremberg, Germany.
- Tamura, S., Anda, Y., Ishida, M., Uemoto, Y., Ueda, T., Tanaka, T. and Ueda, D. (2010). Recent Advances in GaN Power Switching Devices. In: *IEEE Compound Semiconductor Integrated Circuit Symposium*, Monterey, CA, USA.
- Uemoto, Y., Morita, T., Ikoshi, A., Umeda, H., Matsuo, H., Shimizu, J., Hikita, M., Yanagihara, M., Ueda, T., Tanaka, T. and Ueda D. (2009). GaN Monolithic Inverter IC Using Normally-Off Gate Injection Transistors with Planar Isolation on Si Substrate. In: *IEEE International Electron Devices Meeting*, Baltimore, MD, USA.
- Ulmer, S., Schullerus, G. and Sönmez, E. (2021a) Active Damping in Series Connected Power Converters with Continuous Output Voltage. In: *19th International Power Electronics and Motion Control Conference*, Gliwice, Poland.
- Ulmer, S., Schullerus, G. and Sönmez, E. (2021b) Active Filter Damping for a GaN-Based Three Phase Power Stage with Continuous Output Voltage. In: *23rd European Conference on Power Electronics and Applications*, Ghent, Belgium.
- Ulmer, S., Schullerus, G. and Sönmez, E. (2019). A Modular and Scalable Power Electronics Device for the Control of Electric Drives. In: *20th International Symposium on Power Electronics*, Novi Sad, Serbia.